

Performance assessment of the gPLUTO code for the numerical modeling of radio galaxy evolution

Gourab Giri^a, Andrea Mignone^b, Alessio Suriano^{b,c,d}, Marco Rossazza^b, Stefano Truzzi^b

^a*Istituto Nazionale di Astrofisica (INAF) – Istituto di Radioastronomia (IRA), via Gobetti 101, Bologna, 40129, Italy*

^b*Dipartimento di Fisica, Università degli Studi di Torino, Via Pietro Giuria 1, Torino, 10125, Italy*

^c*INAF - Istituto Nazionale di Astrofisica, Osservatorio Astrofisico di Torino, Strada Osservatorio, 20, Pino Torinese, 10025, Italy*

^d*ICSC - Italian Research Center on High Performance Computing, Big Data and Quantum Computing, via Magnanelli, 2, Casalecchio di Reno, 40033, Italy*

Abstract

High-resolution tri-axial simulations are indispensable for realistically co-modeling the dynamical signatures and the radiative fingerprints of astrophysical jets, which are becoming increasingly important in modern computational studies of jet physics. However, such simulations impose extreme computational requirements that often exceed the capabilities of conventional CPU-based codes. GPU-accelerated simulations offer a transformative solution to mitigate these limitations. In this work, we present a detailed performance benchmarking of the recently developed GPU-enabled PLUTO code (gPLUTO), demonstrating runtime speed-ups ranging from an order of magnitude to (approximately) over 30 relative to CPU-only configurations. A direct comparison between computations of extragalactic jet propagation performed at different grid resolutions confirm the physical fidelity and production readiness of the gPLUTO code, while underscoring the importance of resolving the jet radius adequately to capture the jet dynamics accurately. Leveraging GPU-PLUTO's capabilities, we finally present an application by performing high-resolution simulations of giant radio galaxy jets (GRGs $\gtrsim 1$ Mpc), representing the first such well-resolved 3D study to our knowledge (resolving scales down to 500 pc). These simulations probe a range of environmental effects on GRG jets, clarifying their formation from central galaxies within host cosmic structures, rapid peripheral expansion, and the development of asymmetric cocoon morphologies.

Keywords: Relativistic jets, galaxies: groups: general, Methods: numerical, GPU computing, Magnetohydrodynamics (MHD)

1. Introduction

Following the early exploration of extragalactic jets via synchrotron radiation in the 1950s (e.g., [Jennison and Das Gupta, 1953](#)), the field underwent a transformative expansion in the 1970s, as reflected in a new wave of discoveries and systematic observations. This period marked not only the identification of multiple distinct classes of radio jets but also the development of statistical catalogs (e.g., X-shaped radio galaxies ([Hogbom, 1979](#)), giant radio galaxies ([Willis et al., 1974](#)), and other bent or peculiar sources ([Ekers et al., 1978](#))). The growing diversity in observed jet propagation mechanisms highlighted the need for theoretical frameworks capable of testing and extending the standard jet paradigm (cf. [Hardcastle and Croston, 2020](#)). Early efforts focused on simplified analytical models, often restricted to one-dimensional treatments (e.g., [Hjellming and Johnston, 1981](#); [Gower et al., 1982](#)). However, assumptions such as constant parameter evolution (e.g., assuming a steady jet-head advance speed across diverse propagation scales) and the inability to reproduce the observed asymmetric and complex morphologies (jet regimes shaped by jet–environment coupling), soon revealed the limitations of such approaches. These shortcomings drove the field toward numerical simulations, enabling a more realistic exploration of the physical processes governing radio galaxy evolution (cf. [Ferrari, 1998](#)).

The early phase of numerical modeling in this field began in

the late 1980s, focusing primarily on 2D simulations of astrophysical jets ([Norman et al., 1982](#); [Stone and Norman, 1992, 1993](#)). However, it was soon recognized that 2D setups could not fully capture the complex evolution inherent to jets ([Stone and Norman, 1994](#); [Norman, 1996](#)), leading to significant differences compared to full 3D simulations (see also, [Mignone et al., 2010](#)). This realization established a crucial numerical benchmark (requirements of full three-dimensional simulations) that has guided subsequent simulation efforts ever since ([Hardee et al., 2001](#); [Nakamura et al., 2001](#)). While newly developed numerical techniques are often initially tested in 2D for computational efficiency ([Mignone and Bodo, 2006](#); [Vaidya et al., 2018](#); [Kundu et al., 2022](#)), accurately capturing the dynamics of realistic cosmic jets demands full 3D implementation.

As numerical simulations of extragalactic jet propagation continue to advance (cf. [Martí, 2019](#)), the importance of achieving high spatial resolution has become increasingly evident, especially to resolve the jet injection region with an adequate number of grid cells. In fact, high resolution not only improves the fidelity of jet propagation dynamics ([Costa et al., 2025](#)) but also enables the accurate treatment of magneto-hydrodynamical (MHD) instabilities ([Wang et al., 2023](#)), entrainment processes ([Rossi et al., 2024](#)), and the influence of ambient medium tri-axiality on jet evolution ([Hodges-Kluck and Reynolds, 2011](#)). Past studies have indicated that resolving at least eight to ten

grid cells across the jet radius is necessary to capture the key dynamical features of jet propagation (Stone and Norman, 1994; Norman, 1996; Aloy et al., 1999). However, more modern works (Mignone et al., 2010; Hodges-Kluck and Reynolds, 2011; Giri et al., 2022a) demonstrated that increasing the resolution further to have ~ 15 grid cells within the jet radius substantially improves the fidelity of the simulations, enabling a more accurate representation of transverse structures (to the flow), shock formation along the jet beam, and pressure-driven morphological evolution.

In the current era, numerical simulations are becoming increasingly capable of modelling both jet propagation dynamics and their associated non-thermal radiative signatures in a self-consistent manner. This progress has been enabled by advanced Lagrangian–Eulerian particle–fluid techniques (e.g., Mignone et al., 2018; Ogrodnik et al., 2021), which allow the production of synthetic emission maps that can be directly compared with contemporary observational data (e.g., Vaidya et al., 2018; Yates-Jones et al., 2022).

By allowing macro-particles (an ensemble of non-thermal particle distribution following a power-law) to track processes such as particle re-acceleration and cooling, these methods offer a powerful framework to link the jet dynamics with the observable non-thermal emission. Such approaches are in growing demand, not only to address modern questions surrounding radio galaxies (e.g., see, Giri et al., 2022b; Shabala et al., 2024; Dubey et al., 2024), but also to refine our broader understanding of jet microphysics and the mechanisms governing their radiative fingerprints (cf. Pe’er, 2014).

Incorporating this suite of physical processes is both timely and essential for capturing the full complexity of jet–environment interactions. However, doing so drives simulations into a regime of unprecedented computational demand, rapidly exceeding the capabilities of traditional CPU-based codes. A recent study by Dubey et al. (2023) has shown that reliable emission modeling requires a resolution of roughly 25 grid cells per jet radius—a level of detail that, while feasible for compact or galactic-scale jets (tens of kpc), becomes increasingly prohibitive for classical doubles (hundreds of kpc; cf. Saikia, 2022) and giant radio galaxies (>700 kpc; cf. Dabhade et al., 2023). As a result, many CPU-based studies have been forced to compromise: either truncating their models to the early phases of jet evolution (Mukherjee et al., 2021) or reducing the physical realism by omitting key microphysical processes (Giri et al., 2025b). This growing resolution–physics bottleneck highlights an urgent need for next-generation numerical approaches capable of handling both scale and complexity without compromise.

GPU-accelerated codes represent a crucial step in this transition, offering the ability to sustain both high spatial resolution and rich physical complexity over unprecedented spatiotemporal domains (see also, Stone et al., 2024; Liska et al., 2022). By exploiting massively parallel architectures, these frameworks deliver significant speedups over conventional CPU-based approaches, enabling detailed simulations of multi-Mpc jets (e.g., the observed systems of Andernach and Brügggen, 2025) without compromising physical realism. Codes such as gPLUTO

(the GPU-accelerated successor to the widely used PLUTO legacy MHD code; Mignone et al., 2007) exemplify this new generation of numerical tools—poised to bridge the gap between small-scale, well-resolved jet models and realistic large-scale evolutionary scenarios, which will be discussed in this work.

In Section 2, we provide a brief overview of gPLUTO and outline its implementation for simulating systems ranging from classical doubles to giant radio galaxies. Section 3 begins with a performance benchmarking analysis (§ 3.1), comparing gPLUTO (on GPUs) with its CPU counterpart, followed by an investigation of jet dynamics across varying resolutions (§ 3.2). We then present a scientific application to giant radio galaxies—a domain where high-resolution 3D simulations remain exceedingly rare (§ 3.3). Finally, in Section 4, we summarize the key results and implications of this study.

2. Governing equations and numerical implementations

We first provide a concise overview of the physical model in the gPLUTO code, outlining its core principles and governing equations. We then describe the setup of our astrophysical jet simulations and establish the primary scientific objectives of this work. The present paper is not intended as a code-description paper, but rather as a science application and science-readiness demonstration of gPLUTO in the context of large-scale relativistic jet propagation. A detailed description of the GPU-oriented implementation, code architecture, and performance scaling of the fluid module is provided in Rossazza et al. (2026), which constitutes the foundational gPLUTO paper. The development and validation of the particle framework are described in Suriano et al. (*submitted*).

2.1. Equation models in the gPLUTO

The density of a relativistic flow in the observer frame is defined as $D = \gamma\rho$, where ρ is the comoving rest-mass density and γ is the Lorentz factor corresponding to the bulk velocity of the flow. We adopt a Cartesian coordinate system for our simulations, in which the three-velocity vector is denoted by \mathbf{v} . The covariant magnetic field four-vector is expressed as $b^\mu = [b^0, \mathbf{b}] = [\gamma\mathbf{v} \cdot \mathbf{B}, \mathbf{B}/\gamma + \gamma(\mathbf{v} \cdot \mathbf{B})\mathbf{v}]$, where \mathbf{B} is the magnetic field measured in the observer’s frame. The total (gas plus magnetic) pressure of the system is given by $P_t = P_g + \mathbf{B}^2/2\gamma^2 + (\mathbf{v} \cdot \mathbf{B})^2/2$, where P_g denotes the gas pressure. Using these definitions, the total enthalpy can be written as $w_t = \rho h + \mathbf{B}^2/\gamma^2 + (\mathbf{v} \cdot \mathbf{B})^2$, with h representing the specific enthalpy of the relativistic gas. The momentum density is then defined as $\mathbf{m} = w_t\gamma^2\mathbf{v} - b^0\mathbf{b}$, and the total energy density as $E_t = w_t\gamma^2 - (b^0)^2 - P_t$. We further define I as the identity matrix.

With these definitions, the governing equations for a relativistic magnetized gas, as solved in our simulations, are therefore formulated under the assumption of an ideal RMHD framework employing the Taub–Mathews equation of state (Taub, 1948; Mignone et al., 2007), as,

$$\frac{\partial}{\partial t} \begin{pmatrix} D \\ \mathbf{m} \\ E_t \\ \mathbf{B} \end{pmatrix} + \nabla \cdot \begin{pmatrix} D\mathbf{v} \\ w_t \gamma^2 \mathbf{v}\mathbf{v} - \mathbf{b}\mathbf{b} + IP_t \\ \mathbf{m} \\ \mathbf{v}\mathbf{B} - \mathbf{B}\mathbf{v} \end{pmatrix}^T = \begin{pmatrix} 0 \\ \mathbf{f}_g \\ \mathbf{v} \cdot \mathbf{f}_g \\ 0 \end{pmatrix}, \quad (1)$$

where, \mathbf{f}_g is an acceleration term (e.g., due to gravity).

The gPLUTO code is the GPU-accelerated C++ re-design (Rossazza et al., 2026) of the widely used PLUTO legacy code (Mignone et al., 2007) for astrophysical fluid dynamics by means of the OpenACC¹ and OpenMP programming models. In this approach, loops are decorated with compiler directives that instruct the compiler on how to target GPU execution, leaving the low-level handling of threads, memory management, and scheduling to the compiler. This design enables the same codebase to be compiled and executed seamlessly on both CPUs (host) and GPUs (device). In gPLUTO, all the computation is executed directly by GPUs, while CPUs manage global control, memory allocation, and I/O operations. In fact, since GPU and CPU operate on their respective dedicated memory spaces in discrete architectures, data transfers are associated with significant overhead. Therefore, to maximally utilize the parallel efficiency provided by GPUs, it is of utmost importance to ensure device data residency at all times, relegating host copies to the greatest extent. In this context, loops and arrays have been designed to achieve coalesced access to memory, which means to ensure that multiple consecutive threads access adjacent memory spaces. On top, multi-GPU domain decomposition is implemented through MPI² with asynchronous communication, enabling efficient data exchange across neighboring subdomains.

We note that the implementation of the relativistic MHD module in gPLUTO adopts the same parallelization strategy as the non-relativistic version presented in Rossazza et al. (2026). Despite the moderately higher per-cell computational cost associated with primitive-variable recovery and flux evaluations, the increased arithmetic intensity leads to equally good (and in some cases improved) GPU performance.

2.2. Simulation setup for jet propagation

In this study, we model the propagation of extragalactic jets within a poor galaxy group. This ambient medium is adopted following Giri et al. (2025a), representing a triaxial galaxy group (see, Fig. 1), parameterized through the core radii a , b , and c , with $a = b = c$ for most cases, corresponding to an effectively spherical medium, and $a \neq b = c$ for one case to investigate the effects of environmental asymmetry on jet propagation. The density distribution is described using a Cartesian form of the generalized King profile,

$$\rho(x, y, z) = \frac{\rho_0}{\left[1 + \left(\frac{x-x_0}{a} \right)^2 + \left(\frac{y-y_0}{b} \right)^2 + \left(\frac{z}{c} \right)^2 \right]^{3\beta/2}}, \quad (2)$$

where $\rho_0 = 0.001 \text{ amu cm}^{-3}$, $\beta = 0.55$ and the core radii a , b , c range between 33 – 66 kpc, producing a virial radius (R_{virial}) of approximately 830 kpc, raising $R_{500} \approx R_{\text{virial}}/2 \approx 415 \text{ kpc}$ (Lovisari et al., 2015). R_{500} is defined as the radius within which the average density of the medium is 500 times the critical density of the Universe at the present epoch. The ambient medium is formulated to be in static equilibrium, where the pressure gradient balances the gravitational force. The pressure (P_g) follows the adopted density profile, and the gravitational acceleration (\mathbf{g}) is obtained from the hydrostatic equilibrium condition:

$$\nabla P_g = \rho \mathbf{g}. \quad (3)$$

We note that the gravitational field is imposed as a fixed external potential and is not evolved self-consistently during the simulation evolution. The parameters x_0 and y_0 define the center of the ambient medium, which is $(0, 0)$ for all cases. However, in one particular case (mentioned later), the center is shifted to $(x_0, y_0) = (0, -600 \text{ kpc})$ to allow the jet to propagate along the edges of the environment. In all simulations, the jet is injected from $(0, 0, 0)$ and flows around the x -axis throughout its evolution.

The jet is injected into the simulation box through a cylindrical nozzle pointing along the positive x -axis, with initial Lorentz factor of $\gamma = 7$, representing a high-powered relativistic jet (Fanaroff-Riley type - II; Fanaroff and Riley, 1974). The jet is light, with a density contrast of 10^{-5} relative to the ambient medium (ρ_0). In this study, we perform two categories of simulations.

The first category consists of jets propagating up to 100 kpc, primarily to test the robustness of the gPLUTO code in GPUs against CPU-based runs. These standard jet propagation extents in a large-scale cosmic environment are used for performance benchmarking. The jet is injected from $(0, 0, 0)$ through a cylinder of radius 1 kpc, corresponding to a jet power of $5.6 \times 10^{44} \text{ erg s}^{-1}$. We perform four resolution variants of this setup, corresponding to 1, 3, 8, and 15 grid cells per jet radius. These are labeled as follows, and the details of these runs are provided in Table 1:

- “G100³”: 1 cell per jet radius;
- “G300³”: 3 cells per jet radius;
- “G800³”: 8 cells per jet radius;
- “G1500³”: 15 cells per jet radius.

The second category of simulations was performed on much larger spatial scales ($\gtrsim 600 \text{ kpc}$ in one-sided jet propagation) to demonstrate the scientific applicability of gPLUTO in modeling giant radio galaxies—a regime where high-resolution, full three-dimensional simulations remain exceedingly scarce. As GRGs are mostly powered by highly energetic jets (Dabhade et al., 2020; Andernach et al., 2021; Simonte et al., 2024), we adopt a jet radius of 2.5 kpc resolved with five grid cells, corresponding to a jet power of $3.5 \times 10^{45} \text{ erg s}^{-1}$.

Three representative cases were explored. The 1st one, labeled “GRG_centre”, models a jet launched from the center of a spherically symmetric environment. The 2nd one,

¹OpenACC: <https://www.openacc.org/>

²MPI: <https://www.mpi-forum.org/>

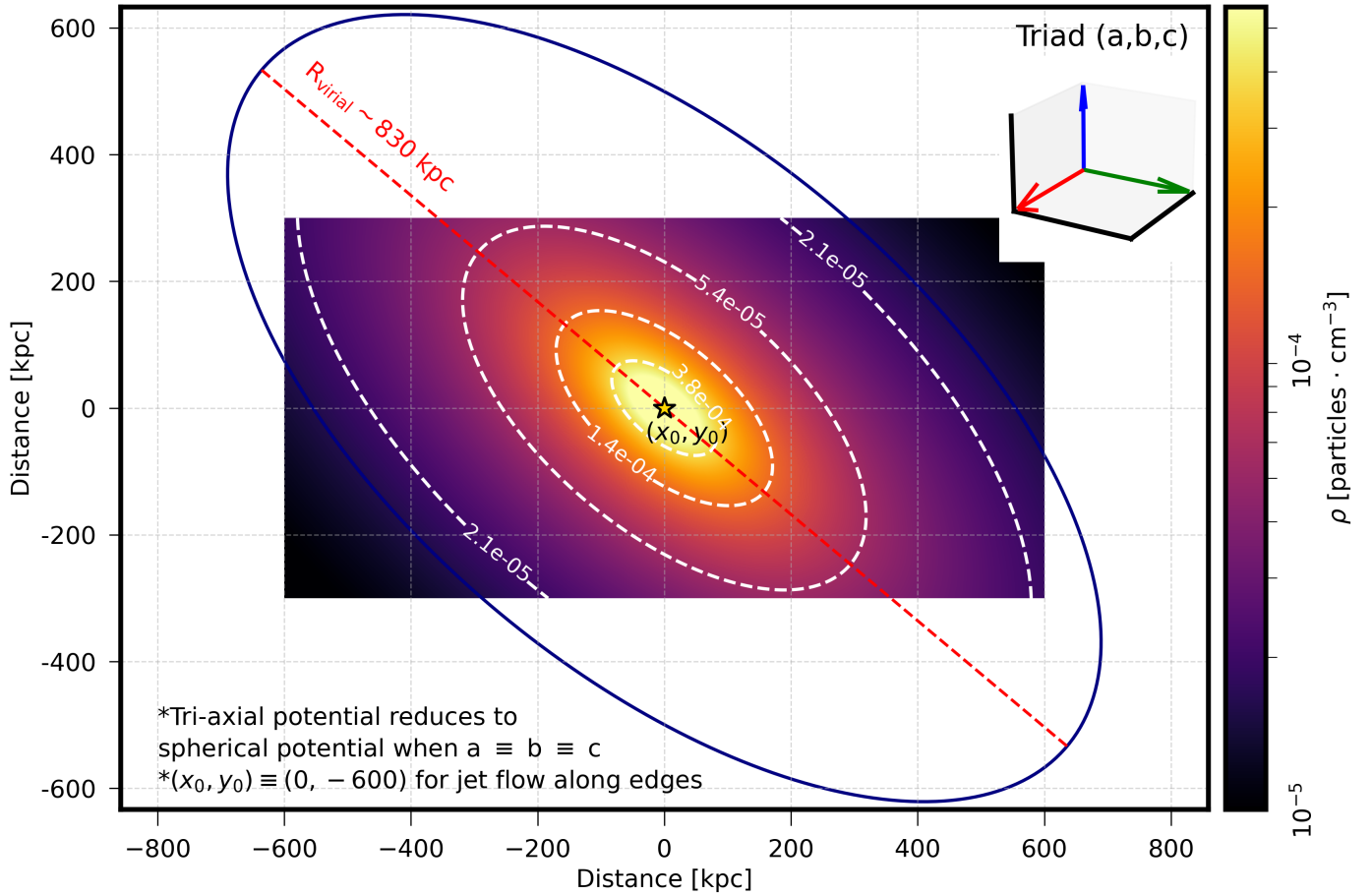


Figure 1: Sliced representation of the triaxial density profile (mimicked through the triad) of a cosmic galaxy group (with core radii a , b , c , and virial radius R_{virial}), representing the ambient medium through which extragalactic jets are injected and propagated in this study. Jets are primarily launched from the center (“GRG_center”), while one case explores injection along the periphery (“GRG_edge”), where the ambient medium is offset by -600 kpc. The tilt of the medium relative to the jet propagation axis (along horizontal path) and its triaxiality demonstrate how we can implement symmetry-breaking in the environment to produce more realistic propagation scenarios (“GRG_asymmetry”). White dashed contour lines, labeled inline, highlight the density stratification relevant to understanding jet-medium interactions.

Runs for performance benchmarking of gPLUTO					
Simulation label	Domain ([X, Y, Z] kpc ³)	Grid cells	Resolution (cells / radius)	Jet radius (kpc)	Jet power (erg · s ⁻¹)
G100 ³	[-10, 100], [-50, 50], [-50, 50]	110 × 100 × 100	1	1.0	5.6 × 10 ⁴⁴
G300 ³	[-10, 100], [-50, 50], [-50, 50]	330 × 300 × 300	3	1.0	5.6 × 10 ⁴⁴
G800 ³	[-10, 100], [-50, 50], [-50, 50]	880 × 800 × 800	8	1.0	5.6 × 10 ⁴⁴
G1500 ³	[-10, 100], [-50, 50], [-50, 50]	1650 × 1500 × 1500	15	1.0	5.6 × 10 ⁴⁴
Runs for scientific applicability of gPLUTO					
Simulation label	Domain ([X, Y, Z] kpc ³)	Grid cells	Resolution (cells / radius)	Jet radius (kpc)	Jet power (erg · s ⁻¹)
GRG_center	[-5, 995], [-160, 160], [-160, 160]	2000 × 640 × 640	5	2.5	3.5 × 10 ⁴⁵
GRG_edge	[-5, 995], [-160, 160], [-160, 160]	2000 × 640 × 640	5	2.5	3.5 × 10 ⁴⁵
GRG_asymmetry	[-600, 600], [-300, 300], [-300, 300]	2400 × 1200 × 1200	5	2.5	3.5 × 10 ⁴⁵

Table 1: A concise overview of the seven simulation categories performed with gPLUTO. The first four were executed on both GPUs and CPUs to benchmark the gPLUTO’s performance across different hardware configurations (jets extending up to 100 kpc). The remaining three runs were carried out to test the scientific applicability and production readiness of gPLUTO, on GPUs (jets extending to $\gtrsim 600$ kpc in one-sided propagation). Each column is duly labeled.

“GRG_edge”, represents a jet injected near the periphery of the large-scale environment, achieved by shifting the medium’s center to $y_0 = -600$ kpc such that the jet, launched from $(0, 0, 0)$, effectively propagates along the group’s edge. The 3rd case, “GRG_asymmetry”, investigates jet propagation through a triaxial environment where the major axis is tilted by 40° relative to the jet propagation direction (which is positive x -direction for all the cases considered), enabling the study of asymmetric cocoon development (refer to Fig 1).

The simulations are briefly described below and summarized in Table 1 for their parametric details:

- “GRG_center”: jet flows from the center of the (spherical) galaxy group medium;
- “GRG_edge”: jet flows from the edge of the (spherical) galaxy group medium;
- “GRG_asymmetry”: jet flows from the center of the (ellipsoidal) galaxy group medium (major axis inclined by 40° to the jet axis).

We note that in all of our simulations, the jet carries a purely toroidal magnetic field, given by, (Rossi et al., 2017):

$$B_y = B_0 r \sin \phi, \quad B_z = B_0 r \cos \phi, \quad (4)$$

where r and ϕ denote the polar coordinates in the y - z plane, and B_0 sets the overall normalization of the field strength, which is fixed at $15 \mu\text{G}$ in all cases. The choice of a substantial toroidal component is well motivated by modern assumptions (see, e.g., Mignone et al., 2010), where such configurations are commonly invoked to drive jet acceleration and collimation. This particular geometry (in Eq. 4) ensures that the magnetic field strength smoothly rises from zero at the jet axis to its maximum at the beam edge, effectively mimicking realistic magnetized jet launching conditions (see, e.g., Lalakos et al., 2024).

To track the evolution and spatial extent of the jet material, we employ a passive scalar (tracer), which is evolved according to a simple advection equation with the jet. The tracer values range from 1 (indicating a cell fully occupied by jet plasma) to 0 (indicating the absence of jet material), enabling a clear distinction between jet and ambient medium throughout the simulation.

2.3. Computing infrastructure for the simulations

All of our simulations were performed on the Leonardo³ supercomputing system hosted and managed by CINECA (Turisini et al., 2023). Leonardo consists of two main partitions⁴: the Booster partition, equipped with 4 GPUs and 32 CPU cores per node; and the Data-centric General Purpose (DCGP) partition, which provides CPU-only nodes with 112 CPU cores

per node. A concise summary of node- and core-level architectural specifications is provided in Table 2. For benchmarking gPLUTO, we employed the same setup (jet evolution followed up to 100 kpc) with different grid resolutions (see Table 1) to assess performance scaling. Specifically, the benchmark runs were first carried out on the Booster partition using GPUs, followed by equivalent CPU-only runs on the same partition, and finally repeated on the DCGP partition to compare against a higher-end CPU architecture (Table 2). This enabled us to quantify the speedup of GPU acceleration relative to both equivalent and superior CPU resources. The scientific application runs (GRGs; Table 1) were performed on the GPU-based Booster partition of the Leonardo.

3. Results

We now present a performance benchmark between traditional CPU-based simulations and their GPU-accelerated counterparts (Section 3.1), providing a quantitative assessment of runtime gains achieved through GPU acceleration. Section 3.2 presents a systematic optimization and convergence analysis between different simulations performed with GPU and CPU configurations. Furthermore, we demonstrate the application of gPLUTO to model astrophysical scenarios where jet propagation physics remains relatively under-explored (Section 3.3), highlighting its potential to enable more detailed and physically realistic studies.

3.1. Performance benchmarking of (CPU vs GPU) gPLUTO

We present here a detailed runtime comparison of individual jet propagation simulations performed using different versions of the gPLUTO code, all executed on the Leonardo HPC system (see Table 2).

We begin with the lowest resolution setup, $G100^3$, which is intentionally designed as a lightweight validation and entry-level benchmark rather than a production-scale performance test. This configuration is meant to assess code correctness and basic performance trends using minimal computational resources, representative of what a new user might access on a local workstation or small test allocation before scaling to full HPC runs. When executed on a single GPU device, this test completed in approximately 2 minutes, whereas the same problem required more than 170 minutes when run on a single CPU core. While this comparison is not intended to represent a realistic allocation-unit benchmark, it clearly demonstrates the intrinsic computational advantage of GPU offloading for this class of problems.

Next, we consider the $G300^3$ configuration, which we adopt as our baseline resolution. The performance difference between GPU- and CPU-based runs remains substantial. When comparing a single GPU-enabled node (with 4 GPUs) to a full CPU node with 32 cores (partition: Booster), the GPU run exhibits a significant speed-up, reducing the runtime by more than an order of magnitude. Even when benchmarked against a high-end state-of-the-art CPU node with 112 cores on the same HPC (partition: DCGP), the GPU-accelerated run still outperforms it

³CINECA - Leonardo: <https://www.hpc.cineca.it/systems/hardware/leonardo/>

⁴System Architecture: <https://docs.hpc.cineca.it/hpc/leonardo.html>

Partition Name	DCGP	Booster
No. of nodes	1536	3456
CPU model	(Intel Sapphire Rapids) Intel Xeon Platinum 8480+	(Intel Ice Lake) Intel Xeon Platinum 8358
CPU cores per node	112	32
CPU Clock Rate	2.6 GHz	2.0 GHz
Memory	512(8x64) GB DDR5	512 GB DDR4
Compiler / version	g++ (GCC) 8.5.0 20210514 (Red Hat 8.5.0-18)	mpicxx / nvc++ 24.5-1
No. of GPUs per node	–	4
GPU Model	–	NVIDIA Ampere100 custom
GPU Memory	–	(HBM2e) 64 GB

Table 2: Key architectural specifications of the Leonardo supercomputing system (hosted and managed by CINECA), comparing the CPU-based DCGP partition and the GPU-enabled Booster partition. The listed specifications are relevant for interpreting the simulation performance comparisons presented in this work (Table 3).

by a factor of ~ 14 . When compared to the 32-core CPU node configuration, the speed-up factor increases to approximately ~ 32 . These results robustly demonstrate that GPU acceleration is not merely competitive but decisively advantageous for time-critical, high-resolution jet simulations.

A comparison of the final jet morphologies (2D density slices) at 6.52 Myr for “G300³” runs in different resource settings is presented in the inset of the Table 3, providing a visual reference to assess the consistency between configurations. The close resemblance between the outputs of GPU-accelerated and CPU-only simulations validates the gPLUTO implementation.

The remarkable performance gains observed in the lower- and baseline-resolution runs motivated us to further test the capabilities of the code at more conventional resolutions—specifically, the “G800³” case, corresponding to eight grid cells per jet radius. This configuration is computationally demanding and typically enters into a challenging regime for traditional CPU-based simulations. As shown in Table 3, the GPU-accelerated run completed in approximately 5 hours, whereas even with 2.7 times longer wall-clock time, CPU-only runs with 32 cores per node and 112 cores per node were unable to reach the same marker point (i.e., 6.52 Myr). In terms of jet evolution time, the CPU-based runs lagged behind by 3.92 Myr and 1.63 Myr, respectively.

When comparing the achieved marker points of these simulations (Table 3), the GPU-enabled run shows roughly a factor of 4 speedup over the high-core (112) CPU-node configuration (at the third data saving interval, i.e., when the simulations reach 4.89 Myr) and nearly a factor of ~ 7 speedup relative to the 32-core CPU-nodes (at the first data-saving interval i.e., at 1.63 Myr)—a performance gap that is expected to widen as the simulation progresses (as evaluated from other grid distribution cases; Table 3). To contextualize the efficiency of the GPU-based runs and its production readiness, we also include an inset image (2D slice of density) showing the morphological and spatial resemblance between the “G800³” and “G300³” gPLUTO outputs, illustrating that the accelerated performance does not compromise the physical fidelity of the simulations.

Building on these encouraging results, we extended our investigation to assess the performance of gPLUTO for high-resolution simulations with 15 grid cells per jet radius (“G1500³”)—a resolution that meets contemporary require-

ments for detailed dynamical and emission modeling in jet physics. Consistently with the lower-resolution cases, gPLUTO in GPU-enabled nodes continues to significantly outperform even the high-core-count CPU only runs when the same number of nodes is used (refer to Table 3), demonstrating its robustness and scalability for computationally demanding astrophysical simulations.

In summary, our performance benchmarking clearly demonstrates that GPU acceleration delivers a transformative improvement in simulation efficiency for jet propagation studies. Across all tested resolutions—from coarse (“G100³”) to high-resolution (“G1500³”) setups—gPLUTO runs in GPU-enabled nodes consistently outperforms full state-of-the-art CPU-only configurations by factors ranging from approximately an order of magnitude to more than a factor of ~ 30 . These speedups are achieved without compromising the physical accuracy or morphological fidelity of the simulated jets, as confirmed by direct visual and quantitative comparisons. This substantial gain in computational efficiency enables higher-resolution, longer-duration, and more physically sophisticated simulations within feasible wall-clock times, establishing GPU acceleration as a powerful and scalable tool for advancing theoretical modeling of astrophysical jet phenomena.

3.2. Convergence analysis through resolution studies

It is particularly insightful to examine the similarities obtained for 100 kpc jet propagation across different CPU and GPU configurations, each performed at varying resolutions. This comparison not only provides a clearer perspective on the consistency between CPU and GPU results but also underscores the critical role of resolution in accurately modeling astrophysical jet dynamics.

Fig. 2 (left) shows the jet propagation length as a function of dynamical age, measured by the maximum extent where the jet tracer exceeds 10^{-7} , a standard proxy for the jet lobe size (Mukherjee et al., 2020). Fig. 2 (right) shows the temporal evolution of the cocoon’s thermal energy, a genuinely volumetric diagnostic (region with jet tracer $\geq 10^{-7}$) that more faithfully traces the structural evolution of the system—such as global lobe expansion, internal adiabatic compressions, and particle mixing—than the approximate 1-D evolution of the jet length. Comparing runs at the same resolution between CPU-only and

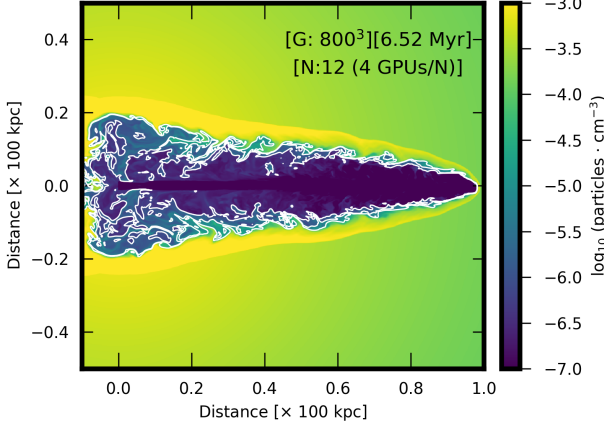
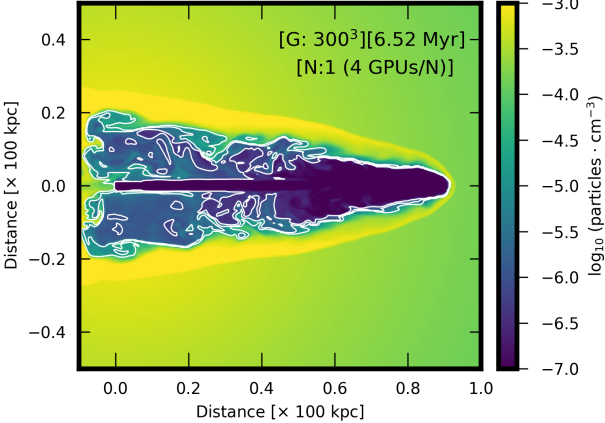
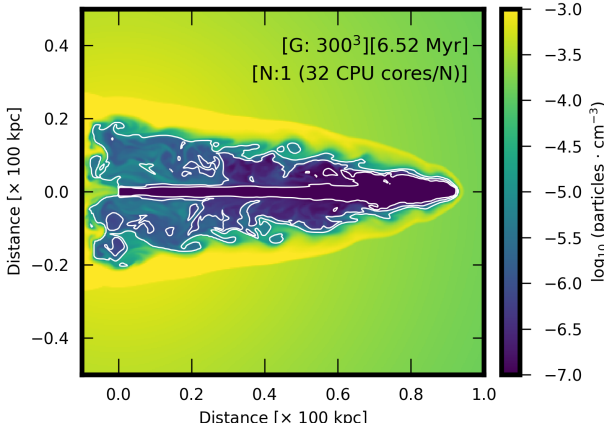
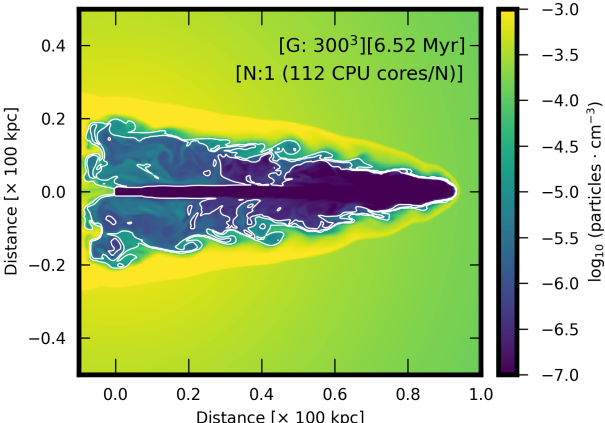
Leonardo – CINECA (Resource specification)	Sim. time (Myr)	[G: 1500 ³] [20 N] Run time (min)	[G: 800 ³] [12 N] Run time (min)	[G: 300 ³] [1 N] Run time (min)	[G: 100 ³] [1 GPU] Run time (min)
GPU partition (Booster) [4 GPUs] /Node	1.63	274.7	69.8	4.48	0.4
	3.26	595.9	127.2	9.75	0.8
	4.89	–	214.6	17.4	1.3
	6.52	–	311.2	27.7	1.9
					
(Resource specification)	Sim. time	[G: 1500 ³] [20 N]	[G: 800 ³] [12 N]	[G: 300 ³] [1 N]	[G: 100 ³] [1 CPU]
GPU partition (Booster) [32 CPU cores] /Node	1.63	–	474.1	110.8	30.2
	3.26	–	888.4* *followed to 2.6 Myr	290.2	71.2
	4.89	–	–	553.8	123.5
	6.52	–	–	894.7	188.4
					
(Resource specification)	Sim. time	[G: 1500 ³] [20 N]	[G: 800 ³] [12 N]	[G: 300 ³] [1 N]	[G: 100 ³] [1 CPU]
CPU partition (DCGP) [112 CPU cores] /Node	1.63	856.4* *followed to 1.2 Myr	158.9	47.1	31.0
	3.26	–	446.4	123.7	73.1
	4.89	–	856.1	233.0	126.4
	6.52	–	–	371.1	194.0

Table 3: Tabular summary of simulations performed with gPLUTO code using different CPU and GPU configurations. *Col. 1* lists the resource setups on the Leonardo HPC system. *Col. 2* shows marker points (data-saving intervals) corresponding to jet evolution time in Myr. *Col. 3–6* give runtimes (minute) to reach each marker for varying grid sizes (G) and node allocations (N). Representative 2D slices from selected runs (green boxes) enable visual comparison. Dashed and asterisks markers denote partially completed runs (followed till a conclusion can be made). Overall, the table highlights the performance advantage of GPU-accelerated PLUTO over (even high-end) CPU-only runs. The last column is visually separated to denote an entry-level validation test performed on a single GPU device versus on a single CPU core.

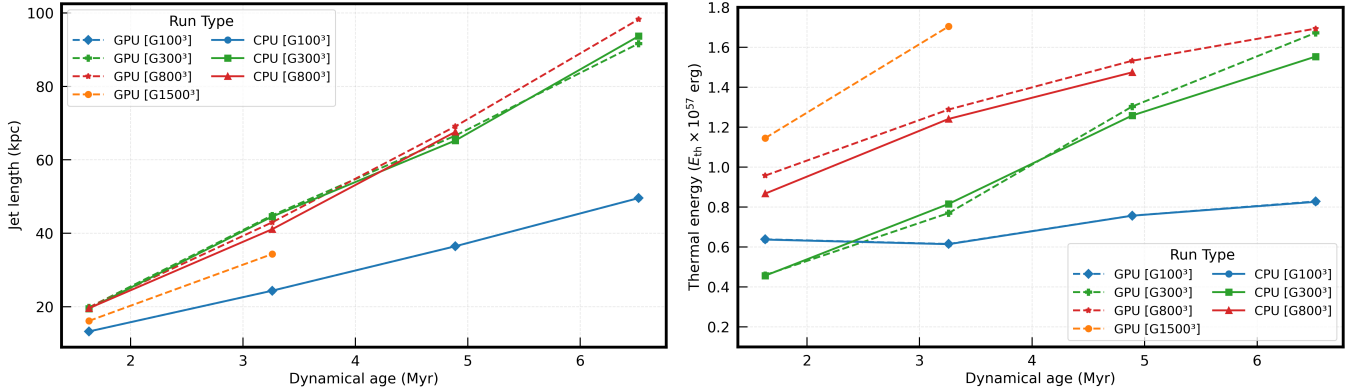


Figure 2: Comparison of gPLUTO CPU-only and GPU simulations showing the jet length evolution as a function of dynamical age (*left*) and the evolution of the thermal energy within the jet cocoon as a function of dynamical age (*right*), highlighting the production readiness of gPLUTO (in GPUs). The plot also illustrates the importance of resolution for accurately capturing jet propagation physics.

GPU-enabled gPLUTO, from $G100^3$ to $G800^3$, reveals a near-identical evolution trajectory.

This demonstrates both the reliability and production readiness of the GPU-accelerated PLUTO code (gPLUTO), while highlighting its significant wall-clock speed-up (Table 3), which substantially enhances the efficiency of magneto-hydrodynamical simulations in jet astrophysics—a domain where PLUTO (legacy code) remained a widely adopted computational tool.

Resolution plays a critical role in accurately capturing jet propagation dynamics, as demonstrated in Fig. 2 (*left*). In the lowest-resolution runs, the jet head exhibits a noticeable lag compared to higher-resolution counterparts, which could lead to misinterpretation of jet evolution. While runs with 3 and 8 cells per jet radius slightly overestimate propagation relative to the 15-cell reference, the differences in these cases are not extreme however. These discrepancies largely reflect how well the simulation resolves the pressure gradients of the ambient medium and the development of magneto-hydrodynamical instabilities within the jet beam and at the cocoon edges (Giri et al., 2025a). Fig. 2 (*right*) presents a more informative diagnostic of the cocoon evolution. The lowest-resolution run fails to reproduce the evolutionary trends observed at higher resolutions, exhibiting only weak temporal variations. For intermediate resolutions (between 3 and 8 cells per jet radius), a modest discrepancy appears during the early stages, reflecting the different ability to resolve the initially compact jet structure between the cases; however, the thermal energy evolution converges at later times as the jet expands. The highest-resolution run (15 cells per jet radius) displays a consistent evolutionary behavior, characterized by a slower expansion rate (see Fig. 2 (*left*)) and correspondingly higher internal pressure within the cocoon.

This analysis underscores the importance of adequately resolving the jet radius and performing convergence tests to ensure reliable and physically meaningful results in jet dynamics simulations.

3.3. Modeling giant radio galaxies with GPU-boostered simulations

Given the substantial reduction in computational time achieved with gPLUTO, it is natural to extend its application to modeling giant radio galaxies—an area where high-resolution simulations remain limited. We have therefore performed simulations at 5 cells per jet radius resolutions for representative giant radio galaxy cases (Table 1), as illustrated in Fig. 3, 4, and 5, to demonstrate the practical applicability and efficiency of GPU-accelerated modeling in this domain.

Fig. 3 shows the propagation of a powerful jet launched from the center of a galaxy group (“GRG_center” case). As it encounters strong environmental resistance, the jet reaches a one-sided distance of ~ 800 kpc in about 19.6 Myr, demonstrating how GRGs with total extents of ~ 1.5 Mpc can originate from central host galaxies, often the brightest members of large-scale cosmic structures (Sankhyayan and Dabhade, 2024). The sustained collimation of the jet at 800 kpc (Fig. 3) indicates its potential for further growth, offering insight into how GRGs larger than 3 Mpc can also emerge from central environments, shedding light on a contemporary finding (Andernach and Brüggén, 2025).

For the case shown in Fig. 4, where the jet is launched from the outskirts of the same galaxy group (~ 600 kpc from the center), the lower environmental resistance allows the jet to reach a distance of ~ 700 kpc in just 6.52 Myr (“GRG_edge” case). Such rapidly propagating jets, if evolved over longer timescales, could likely explain GRGs with remarkable extents up to 5 Mpc or more (Giri et al. *in prep.*). These sources exhibit well-collimated beams enclosed within narrow cocoons—features characteristic of observed GRGs (Machalski et al., 2008; Oei et al., 2024a), relevant to what we have obtained in Fig. 4. The short propagation time obtained in this case (also, see, Jamroz et al., 2008) supports the growing evidence that many GRGs originate or expand along the peripheries of dense cosmic environments (Subrahmanyan et al., 2008), often evolving in filaments or voids (Oei et al., 2024b; Mahato et al., 2025). This scenario aligns with recent observational trends showing a rapid increase in GRG detections

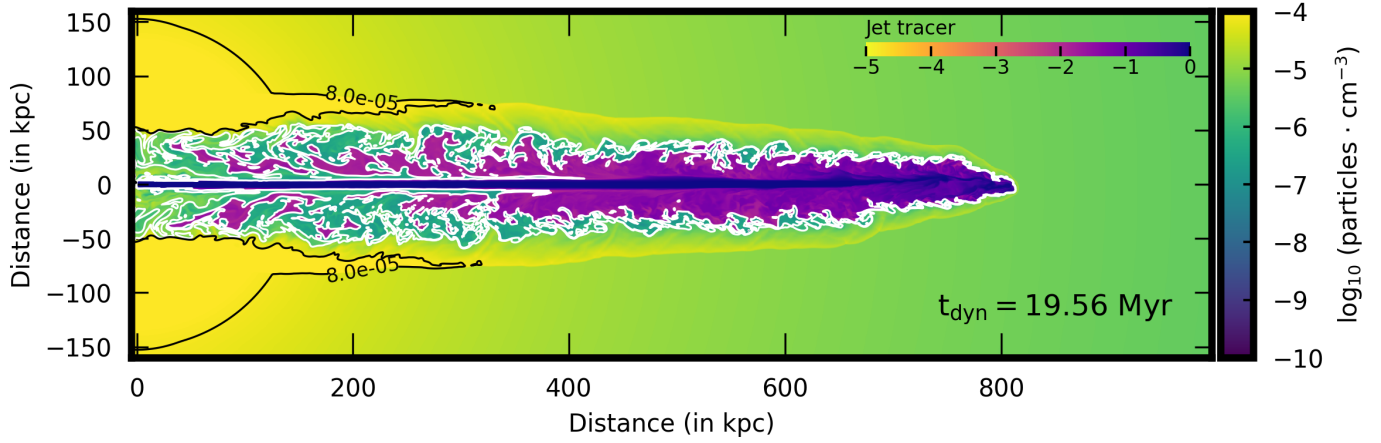


Figure 3: Propagation of a jet reaching giant radio galaxy scales after originating from the center of the large-scale cosmic environment (represented here by a galaxy group, as also inferred by the black density contours). The structure of the jet cocoon is clearly captured using the jet tracer, displayed both as contours (white) and a colormap, and is overplotted on the overall density distribution (all presented in $x-y$ slice at $z = 0$) of the simulated system to illustrate the connection between the jet lobes and the surrounding medium. The evolution time of the simulation is also indicated as inset.

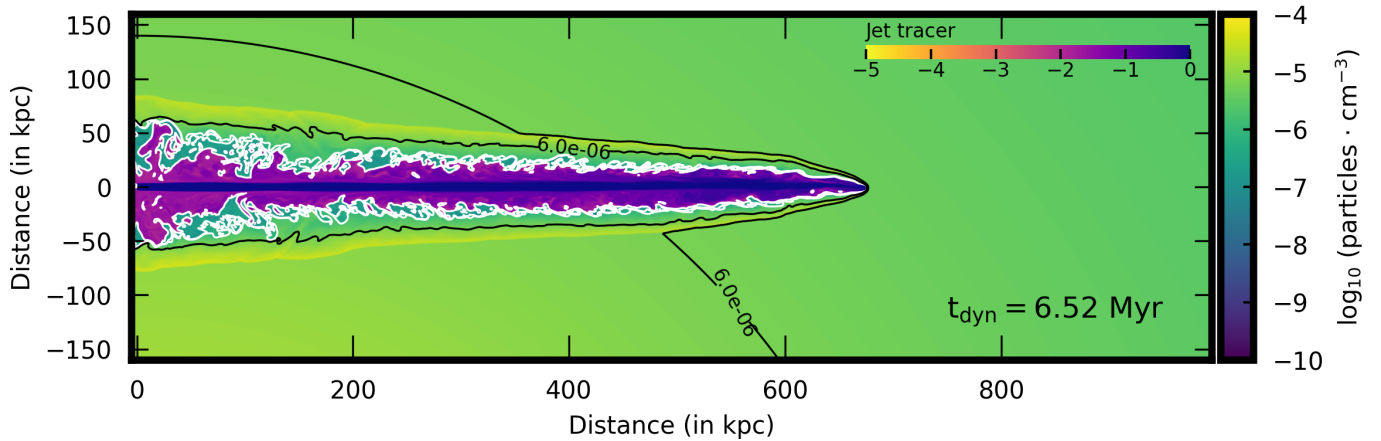


Figure 4: Similar to Fig. 3, but in this case the jet is injected from the outskirts of the large-scale cosmic environment, a configuration often associated with giant radio galaxies. The jet propagates rapidly, reaching approximately 700 kpc in just 6.52 Myr. This fast propagation is important for understanding recent observations of giant jets extending to 5 Mpc and beyond, providing insights into their formation and evolution.

from modern surveys. The inferred sky density of these systems is becoming comparable to that of luminous non-giant radio galaxies (Mostert et al., 2024), indicating that GRGs are not rare or exceptional objects but may in fact be a common population in the radio sky.

To explore GRG evolution in a slightly asymmetric environment, Fig. 5 shows a jet with similar power and density profile as in the previous cases, propagating through a mildly triaxial medium (“GRG_asymmetry” case). The jet reaches ~ 600 kpc in 19.6 Myr, slowed by increased ambient resistance along and around the major axis of the triaxial density distribution. While the overall propagation dynamics resemble Fig. 3, the head advance speed is slightly reduced. Notably, the backflowing plasma (after originating at the jet head due to entropy imbalance, matter backflows; Cielo et al., 2017) at the jet base shows a mild lateral extension along the minor axis due to pressure gradients. In lower-power jets, this backflow could extend further, potentially forming X-shaped morphologies (Capetti et al., 2002; Rossi et al., 2017). These dynamics are relevant for understanding the formation of GRG-XRG systems, which, though rare, are increasingly being observed and characterized in detail (Saripalli and Subrahmanyan, 2009; Cotton et al., 2020; Bruni et al., 2021).

4. Summary

In this work, we have presented an investigation of astrophysical jet propagation using the gPLUTO code, comparing traditional CPU-based simulations with its recently developed GPU-accelerated version. Our performance benchmarks demonstrate that gPLUTO consistently outperforms CPU-only runs across multiple resolutions—from coarse ($G100^3$) to high-resolution ($G1500^3$) setups—achieving speedups ranging from an order of magnitude to approximately over 30 without compromising physical fidelity. These results establish gPLUTO as a production-ready tool for large-scale magneto-hydrodynamical simulations, enabling longer-duration, higher-resolution studies of jet evolution within feasible wall-clock times.

We further analyze convergence of jet simulations through resolution studies, highlighting the critical role of adequate spatial resolution in accurately capturing jet propagation dynamics. Low-resolution runs underestimate key jet dynamics, such as the jet-head advance speed and the evolution of internal energy, potentially misrepresenting the jet evolution, whereas higher-resolution runs converge toward consistent dynamical trajectories.

Following these results, leveraging the computational efficiency of gPLUTO, we model representative giant radio galaxies under various environmental conditions—including central, peripheral, and triaxial host media. These simulations reproduce observed jet morphologies, propagation distances, and cocoon structures, providing insights into extreme GRG formation, collimation maintenance over Mpc scales, and the potential origins of GRG cocoon asymmetries.

Overall, our study underscores the transformative potential of GPU-accelerated simulations, with gPLUTO emerging as a

powerful and scalable tool for modeling relativistic, magnetized astrophysical jets on modern exascale architectures.

Acknowledgements

We acknowledge Istituto Nazionale di AstroFisica (INAF) for awarding this project access and computational time to the LEONARDO supercomputer, owned by the EuroHPC Joint Undertaking, hosted by CINECA (Italy) and the LEONARDO consortium. This paper is supported by the Fondazione ICSC, Spoke 3 Astrophysics and Cosmos Observations and National Recovery and Resilience Plan (Piano Nazionale di Ripresa e Resilienza, PNRR), Project ID CN 00000013 “Italian Research Center on High-Performance Computing, Big Data and Quantum Computing” funded by MUR Missione 4 Componente 2 Investimento 1.4: Potenziamento strutture di ricerca e creazione di “campioni nazionali di R&S (M4C2-19)” - Next Generation EU (NGEU). This work has also received funding from the European High Performance Computing Joint Undertaking (JU) and Belgium, Czech Republic, France, Germany, Greece, Italy, Norway, and Spain under grant agreement No 101093441 (SPACE).

References

- Aloy, M.A., Ibáñez, J.M., Martí, J.M., Gómez, J.L., Müller, E., 1999. High-Resolution Three-dimensional Simulations of Relativistic Jets. *ApJ* 523, L125–L128. doi:10.1086/312266, arXiv:astro-ph/9906428.
- Andernach, H., Brüggén, M., 2025. Properties of giant radio galaxies larger than 3 Mpc. *A&A* 699, A257. doi:10.1051/0004-6361/202452961, arXiv:2505.09181.
- Andernach, H., Jiménez-Andrade, E.F., Willis, A.G., 2021. Discovery of 178 Giant Radio Galaxies in 1059 deg² of the Rapid ASKAP Continuum Survey at 888 MHz. *Galaxies* 9, 99. doi:10.3390/galaxies9040099, arXiv:2111.08807.
- Bruni, G., Brienza, M., Panessa, F., Bassani, L., Dallacasa, D., Venturi, T., Baldi, R.D., Botteon, A., Drabent, A., Malizia, A., Massaro, F., Röttgering, H.J.A., Ubertini, P., Ursini, F., van Weeren, R.J., 2021. Hard X-ray selected giant radio galaxies - III. The LOFAR view. *MNRAS* 503, 4681–4699. doi:10.1093/mnras/stab623, arXiv:2103.00999.
- Capetti, A., Zamfir, S., Rossi, P., Bodo, G., Zanni, C., Masaglia, S., 2002. On the origin of X-shaped radio-sources: New insights from the properties of their host galaxies. *A&A* 394, 39–45. doi:10.1051/0004-6361:20021070, arXiv:astro-ph/0207333.
- Cielo, S., Antonuccio-Delogu, V., Silk, J., Romeo, A.D., 2017. Backflows by active galactic nuclei jets: global properties and influence on supermassive black hole accretion. *MNRAS* 467, 4526–4539. doi:10.1093/mnras/stx403, arXiv:1701.07825.

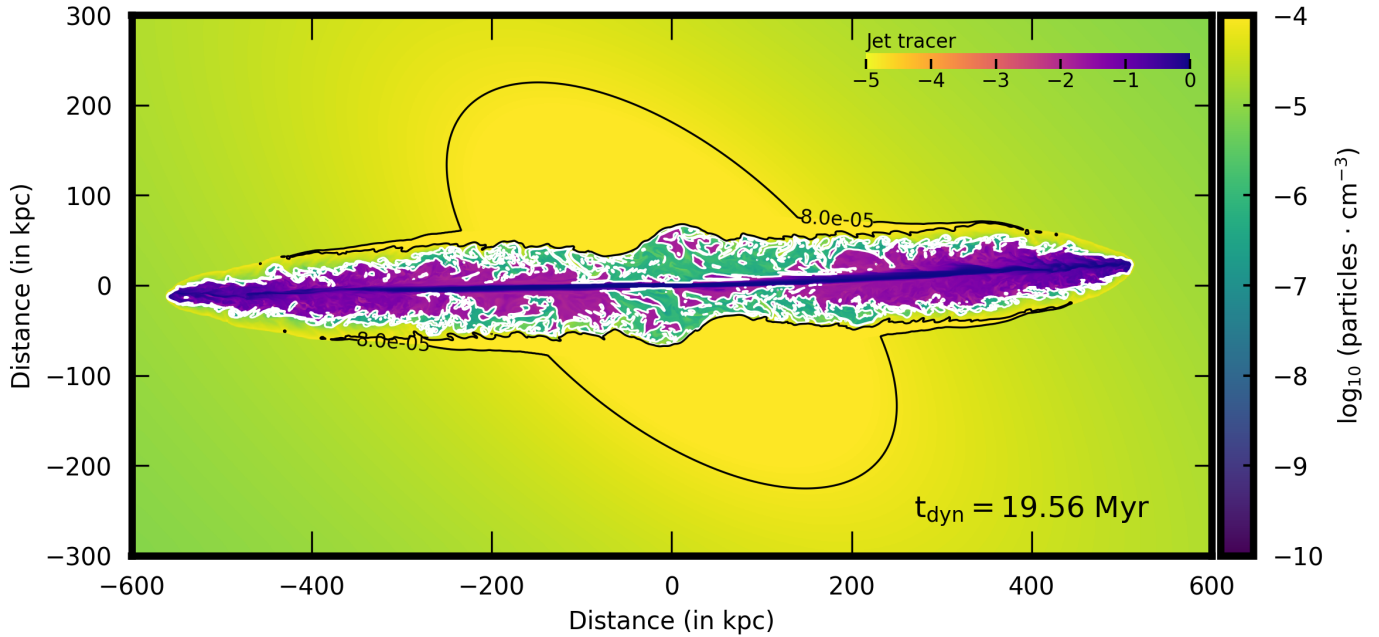


Figure 5: Same as Fig. 3, but in this case the jet is injected from the center of a triaxial medium to examine its propagation under asymmetric environmental conditions. Unlike the previous giant radio galaxy cases, this jet is bidirectional, allowing us to assess the impact of reduced symmetry on the evolution of the system. The propagation speed is slightly lower here due to the increased environmental resistance of the triaxial structure. The limb-like cocoon feature observed in the jet-base region arises from the backflowing plasma preferentially extending along the steepest pressure gradient. Such a feature is expected to become even more prominent in lower power jets, potentially giving rise to complex morphologies such as X-shaped radio galaxies.

- Costa, A., Bodo, G., Tavecchio, F., Rossi, P., Coppi, P., Sciacaluga, A., Boula, S., 2025. How do recollimation-induced instabilities shape the propagation of hydrodynamic relativistic jets? arXiv e-prints, arXiv:2503.18602doi:10.48550/arXiv.2503.18602, arXiv:2503.18602.
- Cotton, W.D., Thorat, K., Condon, J.J., Frank, B.S., Józsa, G.I.G., White, S.V., Deane, R., Oozeer, N., Atemkeng, M., Bester, L., Fanaroff, B., Kupa, R.S., Smirnov, O.M., Mauch, T., Krishnan, V., Camilo, F., 2020. Hydrodynamical backflow in X-shaped radio galaxy PKS 2014-55. MNRAS 495, 1271–1283. doi:10.1093/mnras/staa1240, arXiv:2005.02723.
- Dabhade, P., Röttgering, H.J.A., Bagchi, J., Shimwell, T.W., Hardcastle, M.J., Sankhyayan, S., Morganti, R., Jamrozy, M., Shulevski, A., Duncan, K.J., 2020. Giant radio galaxies in the LOFAR Two-metre Sky Survey. I. Radio and environmental properties. A&A 635, A5. doi:10.1051/0004-6361/201935589, arXiv:1904.00409.
- Dabhade, P., Saikia, D.J., Mahato, M., 2023. Decoding the giant extragalactic radio sources. Journal of Astrophysics and Astronomy 44, 13. doi:10.1007/s12036-022-09898-5, arXiv:2208.02130.
- Dubey, R.P., Fendt, C., Vaidya, B., 2023. Particles in Relativistic MHD Jets. I. Role of Jet Dynamics in Particle Acceleration. ApJ 952, 1. doi:10.3847/1538-4357/ace0bf, arXiv:2306.10902.
- Dubey, R.P., Fendt, C., Vaidya, B., 2024. Particles in Relativistic Magnetohydrodynamic Jets. II. Bridging Jet Dynamics with Multi-wave band Nonthermal Emission Signatures. ApJ 976, 144. doi:10.3847/1538-4357/ad8135, arXiv:2409.15983.
- Ekers, R.D., Fanti, R., Lari, C., Parma, P., 1978. NGC326 - A radio galaxy with a precessing beam. Nature 276, 588–590. doi:10.1038/276588a0.
- Fanaroff, B.L., Riley, J.M., 1974. The morphology of extragalactic radio sources of high and low luminosity. MNRAS 167, 31P–36P. doi:10.1093/mnras/167.1.31P.
- Ferrari, A., 1998. Modeling Extragalactic Jets. ARA&A 36, 539–598. doi:10.1146/annurev.astro.36.1.539.
- Giri, G., Bagchi, J., Thorat, K., Deane, R.P., Delhaize, J., Saikia, D.J., 2025a. Probing the formation of megaparsec-scale giant radio galaxies: I. Dynamical insights from magnetohydrodynamic simulations. A&A 693, A77. doi:10.1051/0004-6361/202451812, arXiv:2411.10864.
- Giri, G., Dubey, R.P., Rubinur, K., Vaidya, B., Kharb, P., 2022a. Dynamical modelling and emission signatures of a candidate dual AGN with precessing radio jets. MNRAS 514, 5625–5639. doi:10.1093/mnras/stac1628, arXiv:2206.04705.
- Giri, G., Fendt, C., Bagchi, J., Thorat, K., Saikia, D.J., Deane, R.P., Delhaize, J., 2025b. Probing the forma-

- tion of megaparsec-scale giant radio galaxies II. Continuum & polarization behavior from MHD simulations. arXiv e-prints , arXiv:2510.03037doi:10.48550/arXiv.2510.03037, arXiv:2510.03037.
- Giri, G., Vaidya, B., Rossi, P., Bodo, G., Mukherjee, D., Mignone, A., 2022b. Modelling X-shaped radio galaxies: Dynamical and emission signatures from the Backflow model. *A&A* 662, A5. doi:10.1051/0004-6361/202142546, arXiv:2203.01347.
- Gower, A.C., Gregory, P.C., Unruh, W.G., Hutchings, J.B., 1982. Relativistic precessing jets in quasars and radio galaxies : models to fit high resolution data. *ApJ* 262, 478–496. doi:10.1086/160442.
- Hardcastle, M.J., Croston, J.H., 2020. Radio galaxies and feedback from AGN jets. *New Astron. Rev.* 88, 101539. doi:10.1016/j.newar.2020.101539, arXiv:2003.06137.
- Hardee, P.E., Hughes, P.A., Rosen, A., Gomez, E.A., 2001. Relativistic Jet Response to Precession and Wave-Wave Interactions. *ApJ* 555, 744–757. doi:10.1086/321525, arXiv:astro-ph/0103224.
- Hjellming, R.M., Johnston, K.J., 1981. An analysis of the proper motions of SS 433 radio jets. *ApJ* 246, L141–L145. doi:10.1086/183571.
- Hodges-Kluck, E.J., Reynolds, C.S., 2011. Hydrodynamic Models of Radio Galaxy Morphology: Winged and X-shaped Sources. *ApJ* 733, 58. doi:10.1088/0004-637X/733/1/58, arXiv:1103.4863.
- Hogbom, J.A., 1979. A study of the radio galaxies 3C 111, 192, 219, 223, 315 and 452. *A&AS* 36, 173–192.
- Jamrozy, M., Konar, C., Machalski, J., Saikia, D.J., 2008. A multifrequency study of giant radio sources - II. Spectral ageing analysis of the lobes of selected sources. *MNRAS* 385, 1286–1296. doi:10.1111/j.1365-2966.2007.12772.x, arXiv:0712.0162.
- Jennison, R.C., Das Gupta, M.K., 1953. Fine Structure of the Extra-terrestrial Radio Source Cygnus I. *Nature* 172, 996–997. doi:10.1038/172996a0.
- Kundu, S., Vaidya, B., Mignone, A., Hardcastle, M.J., 2022. A numerical study of the interplay between Fermi acceleration mechanisms in radio lobes of FR-II radio galaxies. *A&A* 667, A138. doi:10.1051/0004-6361/202244251, arXiv:2208.12823.
- Lalakos, A., Tchekhovskoy, A., Bromberg, O., Gottlieb, O., Jacquemin-Ide, J., Liska, M., Zhang, H., 2024. Jets with a Twist: The Emergence of FR0 Jets in a 3D GRMHD Simulation of Zero-angular-momentum Black Hole Accretion. *ApJ* 964, 79. doi:10.3847/1538-4357/ad0974, arXiv:2310.11487.
- Liska, M.T.P., Chatterjee, K., Issa, D., Yoon, D., Kaaz, N., Tchekhovskoy, A., van Eijnatten, D., Musoke, G., Hesp, C., Rohoza, V., Markoff, S., Ingram, A., van der Klis, M., 2022. H-AMR: A New GPU-accelerated GRMHD Code for Exascale Computing with 3D Adaptive Mesh Refinement and Local Adaptive Time Stepping. *ApJS* 263, 26. doi:10.3847/1538-4365/ac9966, arXiv:1912.10192.
- Lovisari, L., Reiprich, T.H., Schellenberger, G., 2015. Scaling properties of a complete X-ray selected galaxy group sample. *A&A* 573, A118. doi:10.1051/0004-6361/201423954, arXiv:1409.3845.
- Machalski, J., Koziel-Wierzbowska, D., Jamrozy, M., Saikia, D.J., 2008. J1420-0545: The Radio Galaxy Larger than 3C 236. *ApJ* 679, 149–155. doi:10.1086/586703, arXiv:0808.2742.
- Mahato, M., Tempel, E., Sankhyayan, S., Dabhade, P., Chavan, K., 2025. SAGAN-VI: When Jets Meet Filaments – Environmental Imprints on the Growth of Giant Radio Galaxies. arXiv e-prints , arXiv:2512.07985doi:10.48550/arXiv.2512.07985, arXiv:2512.07985.
- Martí, J.M., 2019. Numerical Simulations of Jets from Active Galactic Nuclei. *Galaxies* 7, 24. doi:10.3390/galaxies7010024.
- Mignone, A., Bodo, G., 2006. An HLLC Riemann solver for relativistic flows - II. Magnetohydrodynamics. *MNRAS* 368, 1040–1054. doi:10.1111/j.1365-2966.2006.10162.x, arXiv:astro-ph/0601640.
- Mignone, A., Bodo, G., Massaglia, S., Matsakos, T., Tesileanu, O., Zanni, C., Ferrari, A., 2007. PLUTO: A Numerical Code for Computational Astrophysics. *ApJS* 170, 228–242. doi:10.1086/513316, arXiv:astro-ph/0701854.
- Mignone, A., Bodo, G., Vaidya, B., Mattia, G., 2018. A Particle Module for the PLUTO Code. I. An Implementation of the MHD-PIC Equations. *ApJ* 859, 13. doi:10.3847/1538-4357/aabccd, arXiv:1804.01946.
- Mignone, A., Rossi, P., Bodo, G., Ferrari, A., Massaglia, S., 2010. High-resolution 3D relativistic MHD simulations of jets. *MNRAS* 402, 7–12. doi:10.1111/j.1365-2966.2009.15642.x, arXiv:0908.4523.
- Mostert, R.I.J., Oei, M.S.S.L., Barkus, B., Alegre, L., Hardcastle, M.J., Duncan, K.J., Röttgering, H.J.A., van Weeren, R.J., Horton, M., 2024. Constraining the giant radio galaxy population with machine learning and Bayesian inference. *A&A* 691, A185. doi:10.1051/0004-6361/202348897, arXiv:2405.00232.
- Mukherjee, D., Bodo, G., Mignone, A., Rossi, P., Vaidya, B., 2020. Simulating the dynamics and non-thermal emission of relativistic magnetized jets I. Dynamics. *MNRAS* 499, 681–701. doi:10.1093/mnras/staa2934, arXiv:2009.10475.

- Mukherjee, D., Bodo, G., Rossi, P., Mignone, A., Vaidya, B., 2021. Simulating the dynamics and synchrotron emission from relativistic jets - II. Evolution of non-thermal electrons. *MNRAS* 505, 2267–2284. doi:[10.1093/mnras/stab1327](https://doi.org/10.1093/mnras/stab1327), [arXiv:2105.02836](https://arxiv.org/abs/2105.02836).
- Nakamura, M., Uchida, Y., Hirose, S., 2001. Production of wiggled structure of AGN radio jets in the sweeping magnetic twist mechanism. *New Astron.* 6, 61–78. doi:[10.1016/S1384-1076\(01\)00041-0](https://doi.org/10.1016/S1384-1076(01)00041-0).
- Norman, M.L., 1996. Structure and Dynamics of the 3D Supersonic Jet, in: Hardee, P.E., Bridle, A.H., Zensus, J.A. (Eds.), *Energy Transport in Radio Galaxies and Quasars*, p. 319.
- Norman, M.L., Winkler, K.H.A., Smarr, L., Smith, M.D., 1982. Structure and dynamics of supersonic jets. *A&A* 113, 285–302.
- Oei, M.S.S.L., Hardcastle, M.J., Timmerman, R., Gast, A.R.D.J.G.I.B., Botteon, A., Rodriguez, A.C., Stern, D., Calistro Rivera, G., van Weeren, R.J., Röttgering, H.J.A., Intema, H.T., de Gasperin, F., Djorgovski, S.G., 2024a. Black hole jets on the scale of the cosmic web. *Nature* 633, 537–541. doi:[10.1038/s41586-024-07879-y](https://doi.org/10.1038/s41586-024-07879-y), [arXiv:2411.08630](https://arxiv.org/abs/2411.08630).
- Oei, M.S.S.L., van Weeren, R.J., Hardcastle, M.J., Gast, A.R.D.J.G.I.B., Leclercq, F., Röttgering, H.J.A., Dabhade, P., Shimwell, T.W., Botteon, A., 2024b. Luminous giants populate the dense Cosmic Web. The radio luminosity-environmental density relation for radio galaxies in action. *A&A* 686, A137. doi:[10.1051/0004-6361/202347115](https://doi.org/10.1051/0004-6361/202347115), [arXiv:2404.17776](https://arxiv.org/abs/2404.17776).
- Ogrodnik, M.A., Hanasz, M., Wóltański, D., 2021. Implementation of Cosmic Ray Energy Spectrum (CRESPE) Algorithm in PIERNIK MHD Code. I. Spectrally Resolved Propagation of Cosmic Ray Electrons on Eulerian Grids. *ApJS* 253, 18. doi:[10.3847/1538-4365/abd16f](https://doi.org/10.3847/1538-4365/abd16f), [arXiv:2009.06941](https://arxiv.org/abs/2009.06941).
- Pe'er, A., 2014. Energetic and Broad Band Spectral Distribution of Emission from Astronomical Jets. *Space Sci. Rev.* 183, 371–403. doi:[10.1007/s11214-013-0001-y](https://doi.org/10.1007/s11214-013-0001-y), [arXiv:1306.1355](https://arxiv.org/abs/1306.1355).
- Rossazza, M., Mignone, A., Bugli, M., Truzzi, S., Riha, L., Panoc, T., Vysocky, O., Shukla, N., Romeo, A., Berta, V., 2026. The pluto code on gpus: A first look at eulerian mhd methods. *Astronomy and Computing* 55, 101076. URL: <https://www.sciencedirect.com/science/article/pii/S2213133726000181>, doi:<https://doi.org/10.1016/j.ascom.2026.101076>.
- Rossi, P., Bodo, G., Capetti, A., Massaglia, S., 2017. 3D relativistic MHD numerical simulations of X-shaped radio sources. *A&A* 606, A57. doi:[10.1051/0004-6361/201730594](https://doi.org/10.1051/0004-6361/201730594), [arXiv:1705.07799](https://arxiv.org/abs/1705.07799).
- Rossi, P., Bodo, G., Massaglia, S., Capetti, A., 2024. The different flavors of extragalactic jets: Magnetized relativistic flows. *A&A* 685, A4. doi:[10.1051/0004-6361/202348864](https://doi.org/10.1051/0004-6361/202348864), [arXiv:2402.04707](https://arxiv.org/abs/2402.04707).
- Saikia, D.J., 2022. Jets in radio galaxies and quasars: an observational perspective. *Journal of Astrophysics and Astronomy* 43, 97. doi:[10.1007/s12036-022-09863-2](https://doi.org/10.1007/s12036-022-09863-2), [arXiv:2206.05803](https://arxiv.org/abs/2206.05803).
- Sankhyayan, S., Dabhade, P., 2024. Search and analysis of giant radio galaxies with associated nuclei (SAGAN). IV. Interplay with the Supercluster environment. *A&A* 687, L8. doi:[10.1051/0004-6361/202450011](https://doi.org/10.1051/0004-6361/202450011), [arXiv:2405.19154](https://arxiv.org/abs/2405.19154).
- Saripalli, L., Subrahmanyan, R., 2009. The Genesis of Morphologies in Extended Radio Sources: X-Shapes, Off-Axis Distortions, and Giant Radio Sources. *ApJ* 695, 156–170. doi:[10.1088/0004-637X/695/1/156](https://doi.org/10.1088/0004-637X/695/1/156), [arXiv:0811.1907](https://arxiv.org/abs/0811.1907).
- Shabala, S.S., Yates-Jones, P.M., Jerrim, L.A., Turner, R.J., Krause, M.G.H., Norris, R.P., Koribalski, B.S., Filipović, M., Rudnick, L., Power, C., Crocker, R.M., 2024. Are Odd Radio Circles phoenixes of powerful radio galaxies? *Publ. Astron. Soc. Australia* 41, e024. doi:[10.1017/pasa.2024.11](https://doi.org/10.1017/pasa.2024.11), [arXiv:2402.09708](https://arxiv.org/abs/2402.09708).
- Simonte, M., Andernach, H., Brügger, M., Miley, G.K., Barthel, P., 2024. Giant radio galaxies in the LOFAR deep fields. *A&A* 686, A21. doi:[10.1051/0004-6361/202348904](https://doi.org/10.1051/0004-6361/202348904), [arXiv:2403.08037](https://arxiv.org/abs/2403.08037).
- Stone, J.M., Mullen, P.D., Fielding, D., Grete, P., Guo, M., Kempfski, P., Most, E.R., White, C.J., Wong, G.N., 2024. AthenaK: A Performance-Portable Version of the Athena++ AMR Framework. *arXiv e-prints*, [arXiv:2409.16053](https://arxiv.org/abs/2409.16053)doi:[10.48550/arXiv.2409.16053](https://doi.org/10.48550/arXiv.2409.16053), [arXiv:2409.16053](https://arxiv.org/abs/2409.16053).
- Stone, J.M., Norman, M.L., 1992. ZEUS-2D: A Radiation Magnetohydrodynamics Code for Astrophysical Flows in Two Space Dimensions. I. The Hydrodynamic Algorithms and Tests. *ApJS* 80, 753. doi:[10.1086/191680](https://doi.org/10.1086/191680).
- Stone, J.M., Norman, M.L., 1993. Numerical Simulations of Protostellar Jets with Nonequilibrium Cooling. I. Method and Two-dimensional Results. *ApJ* 413, 198. doi:[10.1086/172988](https://doi.org/10.1086/172988).
- Stone, J.M., Norman, M.L., 1994. Numerical Simulations of Protostellar Jets with Nonequilibrium Cooling. III. Three-dimensional Results. *ApJ* 420, 237. doi:[10.1086/173555](https://doi.org/10.1086/173555).
- Subrahmanyan, R., Saripalli, L., Safouris, V., Hunstead, R.W., 2008. On the Relationship between a Giant Radio Galaxy MSH 05-22 and the Ambient Large-Scale Galaxy Structure. *ApJ* 677, 63–78. doi:[10.1086/529007](https://doi.org/10.1086/529007), [arXiv:0801.3910](https://arxiv.org/abs/0801.3910).

- Taub, A.H., 1948. Relativistic Rankine-Hugoniot Equations. *Physical Review* 74, 328–334. doi:[10.1103/PhysRev.74.328](https://doi.org/10.1103/PhysRev.74.328).
- Turisini, M., Amati, G., Cestari, M., 2023. LEONARDO: A Pan-European Pre-Exascale Supercomputer for HPC and AI Applications. *arXiv e-prints*, arXiv:2307.16885doi:[10.48550/arXiv.2307.16885](https://doi.org/10.48550/arXiv.2307.16885), [arXiv:2307.16885](https://arxiv.org/abs/2307.16885).
- Vaidya, B., Mignone, A., Bodo, G., Rossi, P., Massaglia, S., 2018. A Particle Module for the PLUTO Code. II. Hybrid Framework for Modeling Nonthermal Emission from Relativistic Magnetized Flows. *ApJ* 865, 144. doi:[10.3847/1538-4357/aadd17](https://doi.org/10.3847/1538-4357/aadd17), [arXiv:1808.08960](https://arxiv.org/abs/1808.08960).
- Wang, J.S., Reville, B., Mizuno, Y., Rieger, F.M., Aharonian, F.A., 2023. Particle acceleration in shearing flows: the self-generation of turbulent spine-sheath structures in relativistic magnetohydrodynamic jet simulations. *MNRAS* 519, 1872–1880. doi:[10.1093/mnras/stac3616](https://doi.org/10.1093/mnras/stac3616), [arXiv:2212.03226](https://arxiv.org/abs/2212.03226).
- Willis, A.G., Strom, R.G., Wilson, A.S., 1974. 3C236, DA240; the largest radio sources known. *Nature* 250, 625–630. doi:[10.1038/250625a0](https://doi.org/10.1038/250625a0).
- Yates-Jones, P.M., Turner, R.J., Shabala, S.S., Krause, M.G.H., 2022. PRAiSE: resolved spectral evolution in simulated radio sources. *MNRAS* 511, 5225–5240. doi:[10.1093/mnras/stac385](https://doi.org/10.1093/mnras/stac385), [arXiv:2202.04420](https://arxiv.org/abs/2202.04420).